

# A Hierarchically Nanostructured Cellulose Fiber-Based Triboelectric Nanogenerator for Self-Powered Healthcare Products

Xu He, Haiyang Zou, Zhishuai Geng, Xingfu Wang, Wenbo Ding, Fei Hu, Yunlong Zi, Cheng Xu, Steven L. Zhang, Hua Yu, Minyi Xu, Wei Zhang, Canhui Lu,\* and Zhong Lin Wang\*

Rapid progress in nanotechnology allows us to develop a large number of innovative wearables such as activity trackers, advanced textiles, and healthcare devices. However, manufacturing processes for desirable nanostructure are usually complex and expensive. Moreover, materials used for these devices are mainly derived from nonrenewable resources. Therefore, it poses growing problems for living environment, and causes incompatible discomfort for human beings with long-time wearing. Here, a self-powered cellulose fiber based triboelectric nanogenerator (cf-TENG) system is presented through developing 1D eco-friendly cellulose microfibers/nanofibers (CMFs/CNFs) into 2D CMFs/CNFs/Ag hierarchical nanostructure. Silver nanofibers membrane is successfully introduced into the cf-TENG system by using CMFs/CNFs as template, which shows excellent antibacterial activity. Enabled by its desirable porous nanostructure and unique electricity generation feature, the cf-TENG system is capable of removing PM<sub>2.5</sub> with high efficiency of 98.83% and monitoring breathing status without using an external power supply. This work provides a novel and sustainable strategy for self-powered wearable electronics in healthcare applications, and furthermore paves a way for next-generation flexible, biocompatible electronics.

## 1. Introduction


Flexible electronics, particularly wearable electronics, such as smart watches, e-skins, e-textile devices, etc., have helped sustain the growth of information and technology society in a worldwide

area. Multiple wearables and sensors help human beings interact with other devices and physical environment around them. However, today's consumer electronics have resulted in a growing demand for electronic devices, which inevitably leads to rapid consumption of nonenvironmentally friendly materials and accompanying plenty of electronic waste.<sup>[1]</sup> Consumer electronics which are frequently discarded increase initial cost for the drain on manpower and material resources in landfill, and cause a series of environmental problems.<sup>[2]</sup> Most wearable devices fabricated with man-made materials are vulnerable to a series of problems no matter for long-time wearing on human body or for the environment. Consequently, the incorporation of materials from nature which are nontoxic with renewability and biodegradability, such as cellulose, silk, chitosan, and a variety of other biopolymers, can reduce the accumulation of persistent e-waste when developed as electronic

components/substrates, compatible with human body and benefiting our living environment.<sup>[2b]</sup> Cellulose nanofibers (CNFs), derived from natural resources (bamboo, wood, etc.) with 1D fiber structure,<sup>[3]</sup> have been developed into a series of 2D/3D nanostructures for functional applications, such as anisotropic

Dr. X. He, H. Zou, Dr. X. Wang, Dr. W. Ding, F. Hu, Dr. Y. Zi, Prof. C. Xu, S. L. Zhang, Prof. H. Yu, Prof. M. Xu, Prof. Z. L. Wang  
Department of Materials Science and Engineering  
Georgia Institute of Technology  
Atlanta, GA 30332, USA  
E-mail: zhong.wang@mse.gatech.edu  
Dr. X. He, Prof. W. Zhang, Prof. C. Lu  
State Key Laboratory of Polymer Materials Engineering  
Polymer Research Institute at Sichuan University  
Chengdu 610065, China  
E-mail: canhuilu@scu.edu.cn

Z. Geng  
Department of Chemistry and biochemistry  
Georgia Institute of Technology  
Atlanta, GA 30332, USA  
Dr. Y. Zi  
Department of Mechanical and Automation Engineering  
The Chinese University of Hong Kong  
Shatin, N.T., Hong Kong SAR, China  
Prof. Z. L. Wang  
Beijing Institute of Nanoenergy and Nanosystems  
Chinese Academy of Sciences  
National Center for Nanoscience and Technology (NCNST)  
Beijing 100083, China

 The ORCID identification number(s) for the author(s) of this article can be found under <https://doi.org/10.1002/adfm.201805540>.

DOI: 10.1002/adfm.201805540

foams for strong, superinsulating, and fire-retardant materials,<sup>[4]</sup> ultrathin and highly flexible MXene/CNFs composite paper for electromagnetic interference shielding,<sup>[5]</sup> and conductive Si/CNT/cellulose as flexible anode for Li-ion batteries.<sup>[6]</sup> CNF exhibits considerable advantages in electronics not only for its abundance and biocompatibility, but also lightweight, biodegradability, excellent mechanical properties, and low thermal expansion coefficient ( $CTE < 8.5 \text{ ppm K}^{-1}$ ).<sup>[7]</sup> Therefore, using CNF as a basic component in developing a series of nanostructures for low-cost, environmentally friendly, mechanically flexible, and functional electronic devices has been an attractive choice for next-generation wearable electronics.

With the fast development of the energy-driven society, ambient particulate matter pollution has become one of the most key threats to human health especially in global megacities, due to the high emission amount of pollutants emitted from human activities such as traffic, heat supply, power plants, and industrial processes, leading to a series of respiratory diseases and cardiovascular diseases.<sup>[8]</sup> Among the various hazards of PM pollutants, fine particles ( $PM_{2.5}$ ), which are  $2.5 \mu\text{m}$  in diameter or smaller, are responsible for various allergies and the spread of respiratory diseases.<sup>[9]</sup> The filtration of PM (from micrometer to sub-micrometer) takes longer time and is a complicated task in filter design with desirable porous nanostructures.<sup>[10]</sup> Meanwhile, breathing rate is an important factor that indicates the health status of a person's health, and therefore it is monitored when performing clinical evaluations.<sup>[11]</sup> In view of these issues, a great deal of work has been conducted to improve the health of human body by preventing particulate matter/killing bacteria<sup>[12]</sup> and breathing monitoring.<sup>[13]</sup> However, manufacturing processes for developing desirable nanostructure are usually complex and expensive. Moreover, most of the electronic devices are powered by batteries that need frequent charging, plenty of e-waste, and manpower for replacement, resulting in a series of environmental issues and management problems. Triboelectric nanogenerator (TENG)<sup>[14]</sup> is a newly invented energy-harvesting technology based on triboelectrification and electrostatic induction. Because of its energy conversion efficiency, cost-effectiveness, universal availability, and environmental friendliness, TENG has been developed to drive electronic devices continuously by converting mechanical energy, especially the low-frequency body motion energy, into electric power.<sup>[15]</sup> Previously, a great deal of work has been conducted through developing natural-derived biopolymers (e.g., cellulose, chitin, and chitosan) into self-powered TENG systems, and gratifying results with designed nanostructures and improved performance have been witnessed for a series of self-powered applications.<sup>[16]</sup> However, none of these devices is designed for  $PM_{2.5}$  removal and breathing monitoring. Since developing nanostructure with desirable pores is usually complicated and energy consumption which always accompany with a series of environmental problems, efficient  $PM_{2.5}$  removal is not easy to achieve. Moreover, given the nature of TENG, the electrical output is sensitive to humidity of surrounding environments,<sup>[17]</sup> which becomes a main obstacle when developing hydrophilic cellulose in TENG for breathing monitoring.

Herein, a cellulose fiber based TENG (cf-TENG) simultaneously with  $PM_{2.5}$  removal, antibacterial, and self-powered breathing monitoring were developed, through constructing a

hierarchical nanostructure and utilizing the unique electricity generation of TENG. To create desirable pores, a green, efficient, and versatile method was adopted to introduce 1D biodegradable CNFs into the big pores of cellulose microfibrils (CMFs) skeleton, to form a nanostructured CMFs/CNFs paper. The silver (Ag) nanofibers membrane was then fabricated through using the CMFs/CNFs paper directly as template to finally obtain a CMFs/CNFs/Ag hierarchical 2D nanostructure. The Ag nanofibers membrane was concurrently applied as electrode of the cf-TENG and antibacterial sites. For practical applications, the nanostructured cf-TENG was implanted in a designed two-channel breathing system to assist stable output during breathing. The microstructure, fundamental electric output of the cf-TENG, and consequently resulted  $PM_{2.5}$  removal efficiency, antibacterial activity, and self-powered breathing monitoring were comprehensively studied. Our work provided a green, universal, and high-efficient method for developing hierarchical cf-TENG and demonstrated its excellent effects for improving air quality and breathing monitoring, which indicates our nanostructured cf-TENG has great potential as self-powered wearable electronics for healthcare applications.

## 2. Results and Discussion

### 2.1. Fabrication and Microstructures of the cf-TENG

As is seen in **Figure 1a**, the main idea of our study is to develop an efficient and sustainable method to fabricate a hierarchical nanostructure for cf-TENG, which is further applied for  $PM_{2.5}$  removal, bacteria killing, and self-powered breathing monitoring. The cf-TENG consists of two dielectric layers which are applied as triboelectrification layer that generates triboelectric charges upon contact-separation with each other, and both were deposited with an Ag electrode on the backside. The key element of our material and structure design is the cellulose/Ag hierarchical layer which is composed of nanostructured CNFs, CMFs, and Ag nanolayer. With good flexibility, low thermal expansion coefficient, as well as excellent mechanical properties, CNF is an ideal candidate as an alternative and eco-friendly material as a basic component/substrate for electronic devices.<sup>[5,6,7b]</sup> **Figure 1a** shows the flow diagram of fabricating the hierarchical nanostructure. Detailed fabrication processes for the hierarchical nanostructure are shown in **Figure S1** (Supporting Information). The typical microstructure of a filter paper is shown in **Figure S2a** (Supporting Information). As shown in **Figure 1b**, the CMFs skeleton prepared from filter paper is mainly composed of micropores from several micrometers to several tens of micrometers. CNFs were constructed on both sides of the CMFs paper skeleton to form a unique nanostructure with layers of CNFs on CMFs (**Figure S2b**, Supporting Information). Finally, a nanolayer of Ag was deposited on top surface of the CMFs/CNFs paper. In our design, CNF layers play a key role in constructing a unique hierarchical nanostructure for cf-TENG. CNFs were on one hand used for surface modification of the CMFs paper with a nanostructure, which enhanced the electrification effect of cf-TENG.<sup>[18]</sup> On the other hand, 1D CNFs were also employed on CMFs skeleton to obtain a desirable nanopores-on-micropores 2D structure which was used for

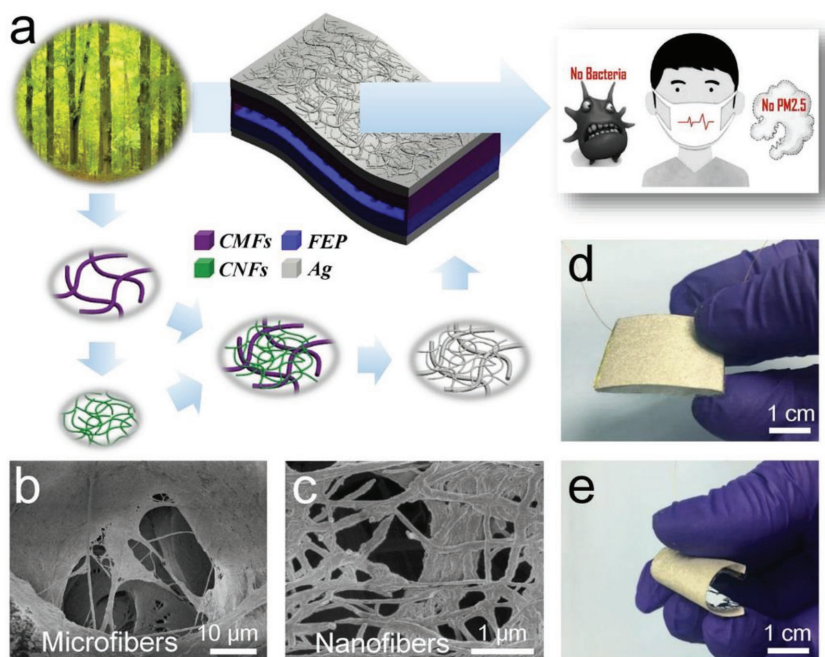


**Figure 1.** Schematic, microstructure, and photographs of the cellulose fiber based triboelectric nanogenerator (cf-TENG). a) Schematic of the cf-TENG, and flow diagram of the fabrication process for cellulose/Ag hierarchical nanostructure, nature-derived 1D cellulose microfibrils (CMFs), and cellulose nanofibers (CNFs) were utilized to develop 2D CMFs/CNFs/Ag hierarchically nanostructured paper for cf-TENG and applied in healthcare products. SEM images show the microstructures of b) CMFs skeleton and c) CMFs/CNFs/Ag paper, respectively. Scale bar: 10 and 1  $\mu\text{m}$ . Photographs of the cf-TENG, d) normal state and e) bent state, scale bar: 1 cm.

particulate matter removal, as will be discussed in later sections. Furthermore, by using CMFs/CNFs paper as template for deposition, a typical nanostructure composed of Ag nanofibers was obtained. This Ag nanofibers membrane was concurrently used as electrode and antibacterial sites. Scanning electron microscopy (SEM) image shows the hierarchical nanostructure of the as-fabricated CMFs/CNFs/Ag membrane (Figure 1c), which depicts a typical nanostructure with nanopores on micropores. Here, UV–visible absorption test on reflectance mode was used to confirm successful deposition of the Ag nanolayer. As seen in Figure S3 (Supporting Information), the CMFs/CNFs sample had no absorption band, however, a broad reflection band was observed around 400 nm due to the surface plasmon resonance of silver nanolayer.<sup>[19]</sup> On the bottom side, a fluorinated ethylene propylene (FEP) film serving as a counter tribo-material was punched with arrays of microholes to assist the breathing air flows through (Figure S4, Supporting Information). Photographs of the as-fabricated cf-TENG at normal state and bent state are shown in Figure 1d,e, respectively. Made of mechanically stable and flexible CMFs/CNFs, cf-TENG has excellent mechanical stability and flexibility which is capable of bending with a high angle (much more than 90°), indicating our cf-TENG has great potential for wearable devices.

## 2.2. Working Principle of the cf-TENG

One of the unique characteristics of our cf-TENG is electricity generation process driven by biomechanical motions.

The self-powered working principle of the cf-TENG can be explained by the coupling effect between contact electrification and electrostatic induction.<sup>[15c]</sup> Due to the large composition percentage of fluorine that enables the highest electronegativity among all elements, the FEP is one of the most triboelectric negative materials, while cellulose tends to gain positive charges when in contact with most of the materials among the triboelectric series.<sup>[20]</sup> In this study, Comsol was employed to simulate the potential distribution of the cf-TENG at open-circuit condition. Operated with an externally applied force triggered by breathing, the two dielectric materials are brought into contact (Figure 2a), surface charge transfer then takes place because of triboelectric effect, with positive ones on cellulose side and negative ones on FEP side.<sup>[20b]</sup> They are balanced by their opposite counterparts, which does not induce an open-circuit voltage across the two electrodes. At the separation state when cellulose paper moves away from FEP layer (Figure 2b), the triboelectric charges do not vanish but remain on the surface of the dielectric layers for a long period of time (Figure 2c),<sup>[21]</sup> an electric potential difference (equivalent to open-circuit voltage,  $V_{oc}$ ) is then established between the two electrodes. It can be expressed by Equation (1) below<sup>[22]</sup>

$$V_{oc} = \frac{\sigma d}{\epsilon_0} \quad (1)$$

where  $\sigma$  is the triboelectric charge density,  $\epsilon_0$  is the vacuum permittivity, and  $d$  is the gap between the two contact dielectric materials. When cellulose layer moves backward, the open-circuit voltage diminishes and drops back to zero when a full contact is made again. In a short-circuit condition, electrons can redistribute between the two back electrodes due to electrostatic induction, which makes net induced charges possible on a single electrode. The induced charge density ( $\sigma'$ ) can be expressed by Equation (2) below<sup>[23]</sup>

$$\sigma' = \frac{\sigma d \epsilon_{rk} \epsilon_{rp}}{d_1 \epsilon_{rp} + d \epsilon_{rk} \epsilon_{rp} + d_2 \epsilon_{rp}} \quad (2)$$

where  $\epsilon_{rk}$  and  $\epsilon_{rp}$  are the relative permittivity of cellulose and FEP,  $d_1$  and  $d_2$  are the thickness of the cellulose paper and the FEP layer, respectively. In a full contact-separation circle at short-circuit condition, the working mechanism is elucidated by four typical states driven by different breathing directions (Figure S5, Supporting Information). The flow of the induced charges then forms output current whose direction relies on contact/separation status of the dielectric layers triggered by different breathing directions. Thus, reciprocating expiration/inspiration motions can produce alternating current (Figure 2d). The electricity generation feature of the self-powered cf-TENG

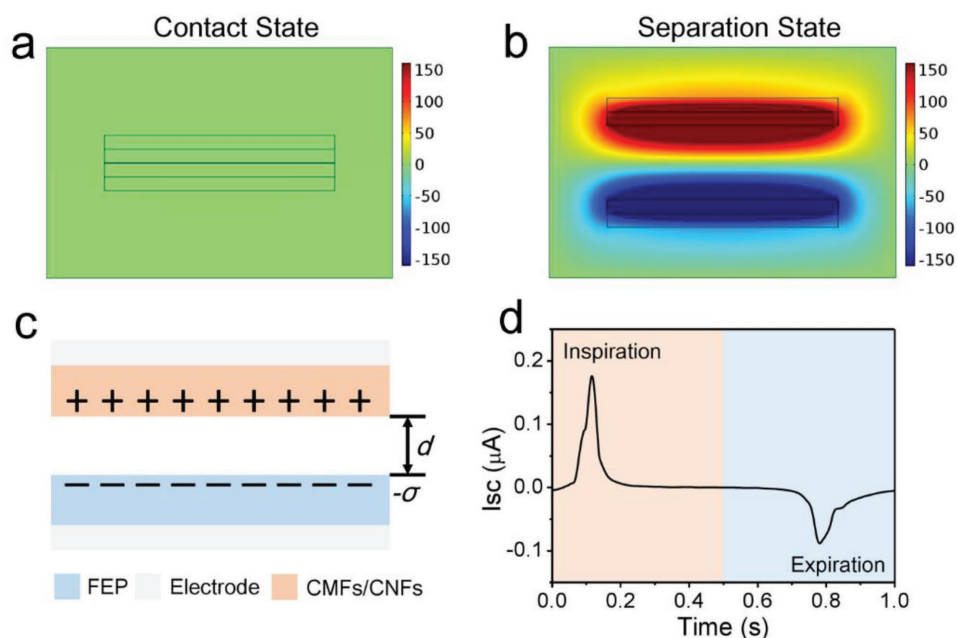


**Figure 2.** Working principle of the cf-TENG. Comsol was employed to elucidate the potential distribution of the cf-TENG at open-circuit condition, a) at the contact state when the FEP layer is in contact with the cellulose layer and b) at the separation state. c) Cross-sectional schematic of the cf-TENG at the separation state. d) Short-circuit current ( $I_{sc}$ ) in a full contact-separation cycle driven by different breathing directions.

is an unparalleled characteristic compared to any other electronic technique.

### 2.3. Electrical Output of the cf-TENG on Different Working Modes

All the unique characteristics of the cf-TENG's electricity generation behavior were experimentally verified by using a linear motor to guide the movement of the dielectric layers between the two electrodes. In this way, the working mode and parameters of the cf-TENG's movement can be accurately controlled. In our study, the electrical output of the cf-TENG is determined by breathing status. Working frequency and displacement of the cf-TENG are two main factors which are influenced by breathing frequency and intensity, respectively. In the first group of experiments, the electrical output performances of the cf-TENG on different working frequencies from 0.5 to 5 Hz were investigated by fixing the working displacement to 3 mm. As seen from **Figure 3a–c**, the open-circuit voltage ( $V_{oc}$ , 21.9 V) and short-circuit charge transfer ( $Q_{sc}$ , 8.3 nC) have almost no change when working frequency varies, while short-circuit current ( $I_{sc}$ ) increases from 0.11 to 0.73  $\mu\text{A}$  with the increase of frequency. This is mainly attributed to the unique characteristics of TENG. Under fixed working displacement,  $V_{oc}$  and  $Q_{sc}$  are mainly determined by the dielectric materials and the structure design of the device. Therefore, both  $V_{oc}$  and  $Q_{sc}$  stay stable with a certain displacement and would not change with different frequencies. At a higher frequency, there are more cycles of charge transfer occurred in a certain time, leading to higher  $I_{sc}$ . In the second group of experiments, the cf-TENG was measured at a fixed working frequency of 1 Hz as a function of operating displacement from 1 to 3 mm. As shown in **Figure 3d–f**, when

the operating displacement increases,  $V_{oc}$ ,  $I_{sc}$ , and  $Q_{sc}$  increase from 2.4 V, 0.01  $\mu\text{A}$ , and 0.4 nC to 21.9 V, 0.17  $\mu\text{A}$ , and 8.3 nC, respectively. This is mainly because the increase of operated displacement between the two dielectric layers enhances the triboelectrification effect of cf-TENG, which results in increase of output performances. Results indicate the electrical output of the cf-TENG depends closely on the operating frequency and displacement, which is unique among electronic devices. For practical application, the output power was further optimized at the external load resistance from 1 to 200  $\text{M}\Omega$ . **Figure S6** (Supporting Information) shows the output voltage and power density of the cp-TENG with an operating gap of 3 mm. At an optimal external load resistance of 20  $\text{M}\Omega$ , peak power density achieves up to 7.68  $\mu\text{W cm}^{-2}$ . The characteristics of the cf-TENG make it ideal for applications which are triggered by mechanical motions, showing great potential in wearable electronics.

### 2.4. Breathing Monitoring and $\text{PM}_{2.5}$ Removal Effect

Since the output value and frequency of cf-TENG rely closely on operating displacement and frequency which are determined by breathing intensity and frequency, it is particularly suitable for breathing monitoring. It should be noted that, given the nature of TENG, the electrical output is sensitive to humidity of surrounding environments, and the electrical output drops by 85% at 95% relative humidity.<sup>[17]</sup> In this study, a breathing system (**Figure S7**, Supporting Information) was designed with two independent channels for expiration and inspiration during breathing, so that the water vapor from expiration will directly flow out and will not influence the electrical output of the cf-TENG. For practical application, the cf-TENG was first assembled with the breathing system

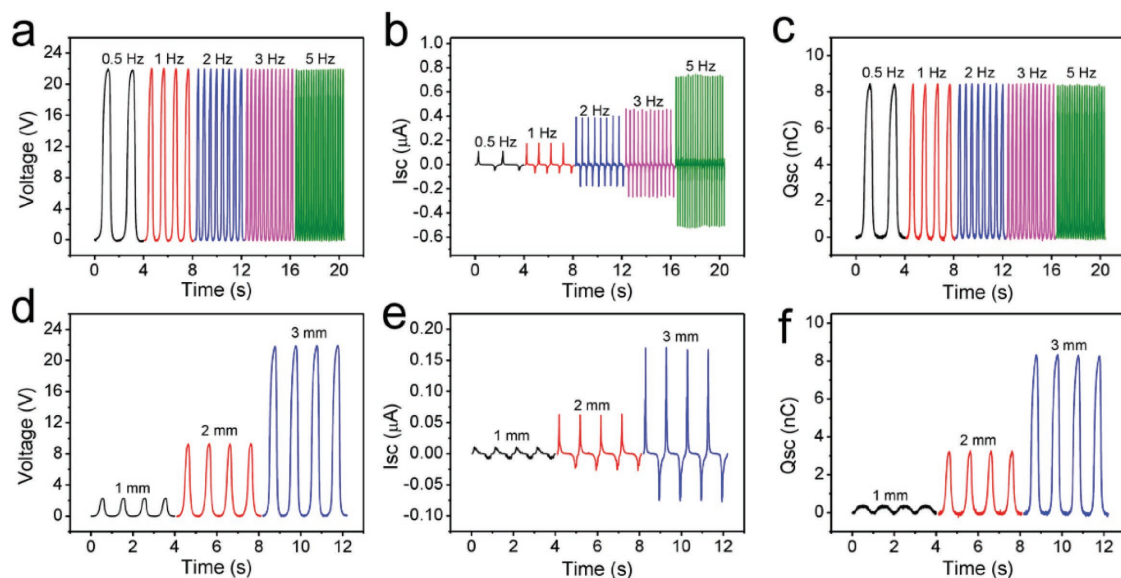


**Figure 3.** The electrical output performance of the cf-TENG on different working frequencies and displacement. a–c) Open-circuit voltage ( $V_{oc}$ )–time curve, short-circuit current ( $I_{sc}$ ), and short-circuit charge transfer ( $Q_{sc}$ ) curve on different frequencies. d–f)  $V_{oc}$ ,  $I_{sc}$ , and  $Q_{sc}$ –time curves on different displacements between the tribo-layers of the TENG.

and then implanted in the mask. **Figure 4a** shows the photograph of the detailed components of the testing system, and the demonstration of electrical signals for the cf-TENG system operated by human breathing. The electrical signal (voltage)

of the cf-TENG was captured with an electrical connection as shown in Figure S8 (Supporting Information). The live demonstration was recorded and shown in Movie S1 (Supporting Information). Through characteristic of TENG, one voltage

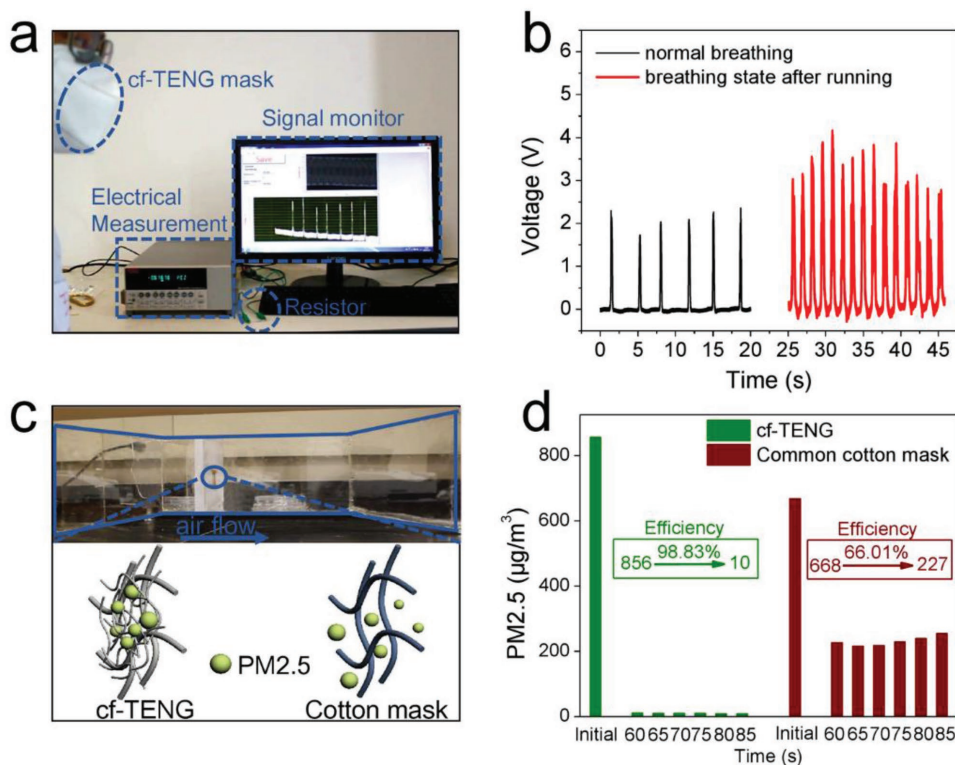


**Figure 4.** Breathing monitoring and  $\text{PM}_{2.5}$  removal effect of the cf-TENG. a) Photograph of the demonstration when the device was implanted in a mask and triggered by human breathing, and detailed components of the testing system. b) Comparative electrical signals for normal breathing and breathing state after running. c) Photograph of the air flow channel (up), and schematic of the cf-TENG (down left) and cotton mask layer (down right) as filtration layer against  $\text{PM}_{2.5}$ . d) Comparative  $\text{PM}_{2.5}$  removal effect between cf-TENG and cotton mask.

peak is produced in one breathing circle, and voltage value is influenced by the operating displacement (Figure 3d). The breathing rate and breathing intensity are determined by the voltage counts (peak counts of the voltage signals) in a certain time and voltage value, respectively. The breathing rate ( $R_b$ ) is calculated by Equation (3) below

$$R_b = \frac{C_v}{t} \quad (3)$$

where  $C_v$  and  $t$  represent the number of voltage counts and the counting time, respectively. As shown in Figure 4b, both the breathing rate and intensity of the tester at normal state are lower than those after running. The breathing rate is calculated to be 15 and 45  $\text{min}^{-1}$  for normal state and the state after a short period of slowly running (5 min), respectively. Voltage values reflected the breathing intensity as summarized in Table S1 (Supporting Information). The fluctuation of the voltage value reflecting the breathing intensity varied from time to time, and the breathing status after running was not so stable as that of the normal state. The average breathing intensity at normal status (2.22 V) is obviously lower than that after running (3.37 V). To confirm the stability of the electrical output for cf-TENG in mask, the electrical output was recaptured after 1 h of normal breathing and followed by a short period of slowly running as shown in Figure S9 and Table S1 (Supporting Information). The breathing intensity shows negligible change after 1 h of normal breathing with a short period of running as compared with that of the original state with short running (3.37 vs 3.47 V), indicating our cf-TENG has excellent electrical stability as wearable electronic device and ideal for breathing monitoring.

Unique characteristics of the cf-TENG are hierarchically nanostructured and mechanical motions triggered electricity generation. As seen in Figure 1c, multilayers of CNFs on CMFs skeleton formed a porous structure with pore sizes less than 1  $\mu\text{m}$ . Therefore, it can be used for protecting a human body against particulate matter from micrometer down to sub-micrometer during breathing. At the same time, particulate matter can be partially eliminated by the electrostatic effect between the dielectric layers of the cf-TENG. However, a common cotton mask cannot effectively protect the human body from  $\text{PM}_{2.5}$  as it generally possesses pores with several tens of micrometers. To elucidate different structures against  $\text{PM}_{2.5}$ , schematic of the porous nanostructure for cf-TENG and the structure for a common cotton mask against  $\text{PM}_{2.5}$  are shown in Figure 4c down left and right, respectively. Here, an air flow channel with two ends open was fabricated to investigate the  $\text{PM}_{2.5}$  removal effect of the cf-TENG (Figure 4 up). An air blower was set at the beginning side of the channel to make sure air flows at a proper speed through the channel. The  $\text{PM}_{2.5}$  removal layer was set in the middle left part of the channel for testing.  $\text{PM}_{2.5}$  removal processes for cf-TENG and cotton mask were compared and recorded in live demonstration in Movies S2 and S3 (Supporting Information). Results were captured every 5 s after 60 s of stable time in  $\text{PM}_{2.5}$  removal process, as shown in Figure 4d and summarized in Table S2 (Supporting Information). For cf-TENG,  $\text{PM}_{2.5}$  value falls rapidly from original 856 down to 10 after 60 s and finally stays at a stable value of 9 after 85 s of  $\text{PM}_{2.5}$  removal process, with an efficiency of 98.83%. However, this value has a different tendency for the

cotton mask. It decreases from 668 to 227 after 60 s and finally stays around 225 after 85 s of  $\text{PM}_{2.5}$  removal process, with an efficiency of 66.01%. Results indicate our cf-TENG has an ultrahigh  $\text{PM}_{2.5}$  removal efficiency which is mainly due to the desirable nanostructure and the triboelectrification effect between the two dielectric layers, showing great potential against  $\text{PM}_{2.5}$ .

## 2.5. Antibacterial Activity of the Nanostructured Membrane

Silver nanoparticles are currently the most widely commercialized nanomaterial which are increasingly used in medical products, due to the strong cytotoxicity toward a broad range of microorganisms.<sup>[24]</sup> In this study, we provide a novel and efficient method to fabricate Ag nanofibers membrane by using CMFs/CNFs membrane as template. The time for deposition of Ag nanolayer is largely reduced to 5 min due to the high surface area of the CMFs/CNFs template, strong bonding interaction between Ag and cellulose fibers.<sup>[19,25]</sup> The antibacterial activity of the as-fabricated CMFs/CNFs/Ag membrane was systematically studied through three sorts of bacteria commonly existing in particulate matter. The concentration of bacteria and killing efficiency of CMFs/CNFs/Ag membrane are summarized in Table 1. Complete sterilization of the original solution occurred at a level of  $\approx 1.2 \times 10^7$  *Escherichia coli* cells killed per  $\text{cm}^2$  of CMFs/CNFs/Ag membrane. As seen in Figure 5a, both cellulose membrane without silver nanolayer and PBS buffer are ineffective against *E. coli* after incubated for 1 h, while CMFs/CNFs/Ag was highly effective against *E. coli* (Figure S10a, Supporting Information). From Figure S10b (Supporting Information), most of the cytotoxic effect was observed after 30 min incubation, and 10 min incubation is not long enough to kill a significant number of bacteria cells. As seen in Figure 5b, when the incubation is extended to 1 h, the growth of up to  $6 \times 10^7$  *E. coli* cells could be inhibited, with killing efficiency up to  $6 \times 10^7$  CFU  $\text{cm}^{-2}$  (Table 1). The excellent antibacterial property of the CMFs/CNFs/Ag membrane is mainly attributed to the Ag nanofibers on the surface, which provides a high specific surface with plenty of antibacterial sites for killing bacteria. Similar levels of cytotoxicity against *Pseudomonas aeruginosa* and *Staphylococcus aureus* are observed from CMFs/CNFs/Ag membrane, with insufficient cytotoxic effect for 10 min and main cytotoxic effect after 30 min (Figure S10c,d, Supporting Information). As shown in Figure 5c,d, after 1 h of incubation, the killing efficiency for *S. aureus* and *P. aeruginosa* achieve up to  $6 \times 10^7$  and  $2.4 \times 10^7$  CFU  $\text{cm}^{-2}$ , respectively (Table 1). Results show the antibacterial activity of nanostructured CMFs/CNFs/Ag membrane is excellent and has great potential in antibacterial applications.

**Table 1.** Antibacterial efficiency after inoculation with *E. coli*, *P. aeruginosa*, and *S. aureus* suspensions incubated with CMFs/CNFs/Ag membrane for 1 h.

Bacteria	<i>E. coli</i>	<i>P. aeruginosa</i>	<i>S. aureus</i>
Initial concentration	$1 \times 10^8$ CFU $\text{mL}^{-1}$	$1 \times 10^8$ CFU $\text{mL}^{-1}$	$1 \times 10^8$ CFU $\text{mL}^{-1}$
1 h concentration	0	0	0
Killing efficiency	$6 \times 10^7$ CFU $\text{cm}^{-2}$	$6 \times 10^7$ CFU $\text{cm}^{-2}$	$2.4 \times 10^7$ CFU $\text{cm}^{-2}$

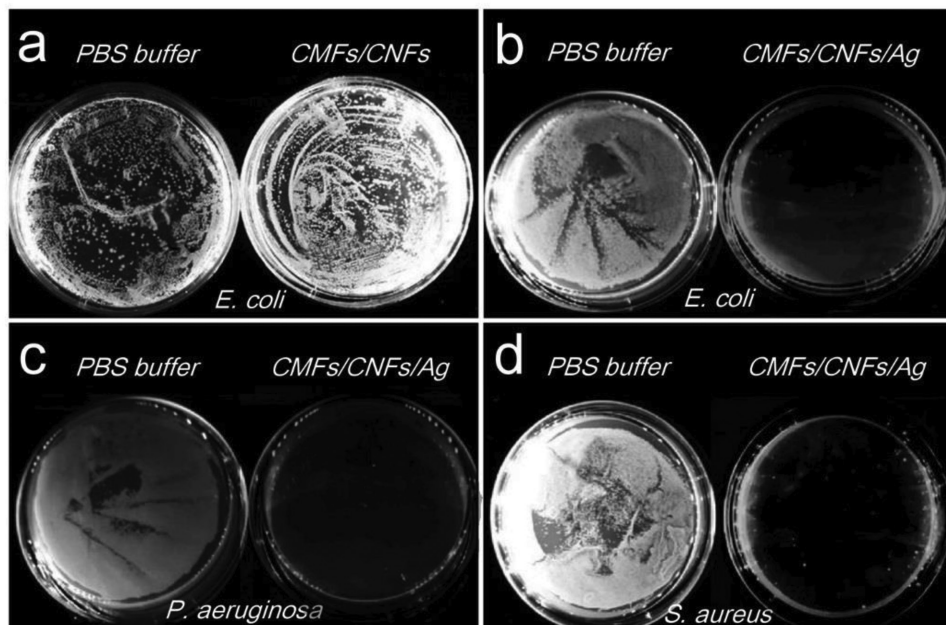


**Figure 5.** Antibacterial activity of the CMFs/CNFs/Ag nanostructured membrane. a) Photographs of agar plates 24 h (37 °C) after inoculation with *E. coli* suspensions incubated with CMFs/CNFs membrane for 1 h (left), and PBS buffer for 1 h (right). b) Photographs of agar plates 24 h (37 °C) after inoculation with *E. coli* suspensions incubated with PBS buffer for 1 h (left) and CMFs/CNFs/Ag membrane for 1 h (right). Demonstration of antibacterial activity against c) *P. aeruginosa* and d) *S. aureus* are incubated with PBS buffer for 1 h (left) and CMFs/CNFs/Ag membrane for 1 h (right), respectively.

### 3. Conclusions

In summary, the feasibility of synergistically removing PM<sub>2.5</sub>, killing bacteria, and monitoring breathing via a single electronic device was established, through the introduction of a hierarchical nanostructure into the self-powered cf-TENG system with a unique electricity generation characteristic. An efficient, low-cost, and sustainable strategy was developed by constructing 1D CNFs on CMFs skeleton to form a desirable 2D hierarchical nanostructure with high efficiency for PM<sub>2.5</sub> removal (98.83%). Meanwhile, a novel and efficient method for fabrication of Ag nanofibers membrane was developed through using CMFs/CNFs as template, which showed excellent antibacterial activity. Breathing rate and intensity were successfully detected via the unique electricity generation dependence of cf-TENG on different operating displacements and frequencies. Our ongoing efforts in materials fabrication and structure design of the cf-TENG would therefore not only provide a new way for wearable electronics in health-care applications, but also lead to a new generation of more eco-friendly, functional, and mechanically flexible electronics that could help decrease the accumulation of electronic waste and dramatically reduce the consumption of nonrenewable resources.

### Supporting Information

Supporting Information is available from the Wiley Online Library or from the author.

### Acknowledgements

X.H. and H.Z. contributed equally to this work. This research was supported by the Hightower Chair foundation and the Thousands Talents programme for pioneer researcher and his innovation team, China, National Natural Science Foundation of China (Grant Nos. 51432005 and 51473100), and State Key Laboratory of Polymer Materials Engineering (sklpme2016-3-09).

### Conflict of Interest

The authors declare no conflict of interest.

### Keywords

breathing monitoring, cellulose nanofibers, eco-friendly electronics, PM<sub>2.5</sub>, triboelectric nanogenerator

Received: August 10, 2018

Published online:

- [1] a) M. Irimia-Vladu, E. D. Głowacki, G. Voss, S. Bauer, N. S. Sariciftci, *Mater. Today* **2012**, *15*, 340; b) Y. H. Jung, T.-H. Chang, H. Zhang, C. Yao, Q. Zheng, V. W. Yang, H. Mi, M. Kim, S. J. Cho, D.-W. Park, *Nat. Commun.* **2015**, *6*, 7170.
- [2] a) B. H. Robinson, *Sci. Total Environ.* **2009**, *408*, 183; b) M. Irimia-Vladu, *Chem. Soc. Rev.* **2014**, *43*, 588.
- [3] H. Zhu, Y. Li, Z. Fang, J. Xu, F. Cao, J. Wan, C. Preston, B. Yang, L. Hu, *ACS Nano* **2014**, *8*, 3606.

- [4] B. Wicklein, A. Kocjan, G. Salazar-Alvarez, F. Carosio, G. Camino, M. Antonietti, L. Bergström, *Nat. Nanotechnol.* **2015**, *10*, 277.
- [5] W. T. Cao, F. F. Chen, Y. J. Zhu, Y. G. Zhang, Y. Y. Jiang, M. G. Ma, F. Chen, *ACS Nano* **2018**, *12*, 4583.
- [6] L. Hu, N. Liu, M. Eskilsson, G. Zheng, J. McDonough, L. Wågberg, Y. Cui, *Nano Energy* **2013**, *2*, 138.
- [7] a) M. Nogi, S. Iwamoto, A. N. Nakagaito, H. Yano, *Adv. Mater.* **2009**, *21*, 1595; b) G. Zheng, Y. Cui, E. Karabulut, L. Wågberg, H. Zhu, L. Hu, *MRS Bull.* **2013**, *38*, 320.
- [8] Z. Cheng, L. Luo, S. Wang, Y. Wang, S. Sharma, H. Shimadera, X. Wang, M. Bressi, R. M. de Miranda, J. Jiang, *Environ. Int.* **2016**, *89*, 212.
- [9] C. Cao, W. Jiang, B. Wang, J. Fang, J. Lang, G. Tian, J. Jiang, T. F. Zhu, *Environ. Sci. Technol.* **2014**, *48*, 1499.
- [10] Y. Chen, S. Zhang, S. Cao, S. Li, F. Chen, S. Yuan, C. Xu, J. Zhou, X. Feng, X. Ma, B. Wang, *Adv. Mater.* **2017**, *29*, 1606221.
- [11] F. Q. AL-Khalidi, R. Saatchi, D. Burke, H. Elphick, S. Tan, *Pediatr. Pulmonol.* **2011**, *46*, 523.
- [12] a) Z. Zhong, Z. Xu, T. Sheng, J. Yao, W. Xing, Y. Wang, *ACS Appl. Mater. Interfaces* **2015**, *7*, 21538; b) S. Jeong, H. Cho, S. Han, P. Won, H. Lee, S. Hong, J. Yeo, J. Kwon, S. H. Ko, *Nano Lett.* **2017**, *17*, 4339.
- [13] a) D. Shen, M. Xiao, G. Zou, L. Liu, W. W. Duley, Y. N. Zhou, *Adv. Mater.* **2018**, *30*, 1870128; b) Z. Zhao, C. Yan, Z. Liu, X. Fu, L. M. Peng, Y. Hu, Z. Zheng, *Adv. Mater.* **2016**, *28*, 10267.
- [14] F.-R. Fan, Z.-Q. Tian, Z. L. Wang, *Nano Energy* **2012**, *1*, 328.
- [15] a) W. Seung, M. K. Gupta, K. Y. Lee, K.-S. Shin, J.-H. Lee, T. Y. Kim, S. Kim, J. Lin, J. H. Kim, S.-W. Kim, *ACS Nano* **2015**, *9*, 3501; b) Y. Zi, H. Guo, Z. Wen, M.-H. Yeh, C. Hu, Z. L. Wang, *ACS Nano* **2016**, *10*, 4797; c) Z. L. Wang, J. Chen, L. Lin, *Energy Environ. Sci.* **2015**, *8*, 2250; d) C. Deng, W. Tang, L. Liu, B. Chen, M. Li, Z. L. Wang, *Adv. Funct. Mater.* **2018**, 1801606.
- [16] a) W. Jiang, H. Li, Z. Liu, Z. Li, J. Tian, B. Shi, Y. Zou, H. Ouyang, C. Zhao, L. Zhao, *Adv. Mater.* **2018**, 1801895; b) Q. Zheng, L. Fang, H. Guo, K. Yang, Z. Cai, M. A. B. Meador, S. Gong, *Adv. Funct. Mater.* **2018**, *28*, 1706365; c) H.-J. Kim, E.-C. Yim, J.-H. Kim, S.-J. Kim, J.-Y. Park, I.-K. Oh, *Nano Energy* **2017**, *33*, 130; d) C. Yao, A. Hernandez, Y. Yu, Z. Cai, X. Wang, *Nano Energy* **2016**, *30*, 103; e) X. Wang, C. Yao, F. Wang, Z. Li, *Small* **2017**, *13*, 1702240.
- [17] J. Chun, J. W. Kim, W.-S. Jung, C.-Y. Kang, S.-W. Kim, Z. L. Wang, J. M. Baik, *Energy Environ. Sci.* **2015**, *8*, 3006.
- [18] a) J. Chen, G. Zhu, J. Yang, Q. Jing, P. Bai, W. Yang, X. Qi, Y. Su, Z. L. Wang, *ACS Nano* **2015**, *9*, 105; b) M. H. Yeh, H. Guo, L. Lin, Z. Wen, Z. Li, C. Hu, Z. L. Wang, *Adv. Funct. Mater.* **2016**, *26*, 1054.
- [19] S. Ifuku, M. Tsuji, M. Morimoto, H. Saimoto, H. Yano, *Biomacromolecules* **2009**, *10*, 2714.
- [20] a) Z. L. Wang, *ACS Nano* **2013**, *7*, 9533; b) A. Diaz, R. Felix-Navarro, *J. Electrostat.* **2004**, *62*, 277.
- [21] J. Wang, S. Li, F. Yi, Y. Zi, J. Lin, X. Wang, Y. Xu, Z. L. Wang, *Nat. Commun.* **2016**, *7*, 12744.
- [22] S. Niu, S. Wang, L. Lin, Y. Liu, Y. S. Zhou, Y. Hu, Z. L. Wang, *Energy Environ. Sci.* **2013**, *6*, 3576.
- [23] G. Zhu, B. Peng, J. Chen, Q. Jing, Z. L. Wang, *Nano Energy* **2015**, *14*, 126.
- [24] L. Rizzello, P. P. Pompa, *Chem. Soc. Rev.* **2014**, *43*, 1501.
- [25] J. He, T. Kunitake, A. Nakao, *Chem. Mater.* **2003**, *15*, 4401.